Microstructural Characteristics of Plasma Nitrided Layer on Hot-Rolled 304 Stainless Steel with a Small Amount of α-Ferrite

XIAOLEI XU, ZHIWEI YU, LIYING CUI, XINJUN NIU, and TAO CAI

The hot-rolled 304 stainless steel with γ-austenite and approximately 5 pct α-ferrite elongated along the rolling direction was plasma-nitrided at a low temperature of 693 K (420 °C). X-ray diffraction results revealed that the nitrided layer was mainly composed of the supersaturated solid solution of nitrogen in austenite (γ_N). Transmission electron microscopy (TEM) observations showed that the microstructure of the γ_N phase exhibited "fracture factor contrast" reflective of the occurrence of fine pre-precipitations in γ_N by the continuous precipitation. The occurrence of a diffuse scattering effect on the electron diffraction spots of γ_N indicated that the pre-precipitation took place in γ_N in the form of strongly bonded Cr-N clusters or pairs due to a strong attractive interaction of nitrogen with chromium. Scanning electron microscopy and TEM observations indicated that the discontinuous precipitation initiated from the γ/α interfaces and grew from the austenite boundaries into austenite grains to form a lamellar structure consisting of CrN and ferrite. The orientation relationship between CrN and ferrite corresponded to a Baker-Nutting relationship: $(100)_{CrN}//(100)_{\alpha}$; $[011]_{CrN}//[001]_{\alpha}$. A zigzag boundary line following the banded structure of alternating γ-austenite and elongated α-ferrite was presented between the nitrided layer and the substrate to form a continuous varying layer thickness, which resulted from the difference in diffusivities of nitrogen in α-ferrite and γ-austenite, along the γ/α interfaces and through the lattice. Microstructural features similar to the γ_N were also revealed in the ferrite of the nitrided layer by TEM. It was not excluded that a supersaturated solid solution of nitrogen in ferrite (α_N) formed in the nitrided layer.

I. INTRODUCTION

MOST stainless steels have relatively low hardness and poor wear-resistance properties. Therefore, a significant amount of research effort has been dedicated to surface modification of the stainless steels. Plasma nitriding has been widely used in industrial production to increase surface hardness and, hence, to improve the wear resistance of ferrous materials. For most austenite stainless steels, reducing the treatment temperature can prevent CrN from precipitating so that a nitrogen supersaturated austenite or expanded austenite γ_N[1–5] can be produced. γ_N has high hardness and wear resistance without compromising the corrosion resistance of the substrate. Knowledge of γ_N is still insufficient with regard to its structure and its stoichiometric chemical composition; therefore, this is a major research focus.[6–9] Specifically, there have been some works on the nitriding of duplex or multiphase stainless steels,[10–14] but most works have focused on single-phase austenitic stainless steels. Complications can arise in duplex-phase or multiphase stainless steels that can contain austenite, ferrite, and martensite. More studies of plasma nitriding of austenite stainless steels showed that the expanded austenite (γ_N) was observed together with Cr-nitride (CrN) at a temperature above 773 K (500 °C) or prolonged treatment.[8] However, the phases present in the nitrided layer, its microstructure, its layer thickness, and its nitrogen concentration not only depend on the processing temperature and time but also on the steel grade, and even more on the phase constitution of the substrate[15,16] due to the significant difference of nitrogen solubilities and diffusivities in ferrite and austenite. Previous studies also suggested that the expanded austenite is not restricted to the austenite stainless steels, but it can also be found in the austenitic-ferrite stainless steels. The stability of the expanded austenite in the austenite-ferritic steel is lower, and the amount of decomposition products (ferrite and CrN) is higher under the same treatment conditions when compared with austenitic stainless steels.[15] In 2205 duplex stainless steel, for example, CrN were found to form from the places where there were ferrite grains when nitrocarburizing at a low temperature of 703 K (430 °C).[10] In the present study, a cellular precipitation reaction in the stainless steel with dual-phases structures

XIAOLEI XU and ZHIWEI YU, Professors, LIYING CUI, Engineer, and XINJUN NIU and TAO CAI, Graduate Students, are with the Department of Materials Science and Engineering, Dalian Maritime University, Dalian, P.R. China. Contact e-mail: 1944816400@qq.com
Manuscript submitted September 24, 2014.
Article published online December 11, 2015.

was observed at low-temperature nitridation [703 K (420 °C)]. Cellular precipitation has been extensively studied in nitrided Fe-Cr alloys,[11] but with regard to stainless steels, there are only limited studies of cellular precipitation reaction. Work on AISI 420 martensitic stainless steel indicated that the nitrided layer retained its martensitic structure at a treatment temperature of 673 K (400 °C) but with a larger lattice parameter than the substrate[17] from their X-ray diffraction (XRD) results, which was identified as "expanded martensite." In present study, an obvious lattice expansion of the nitrided ferrite was not detected by XRD, but XRD may not be capable of resolving all the structural characteristics involved. In this study, the nitrided layer was studied by transmission electron microscopy (TEM), but the microstructures and corresponding electron diffraction patterns (EDPs) that were revealed were complicated and not in full agreement with XRD results. Therefore, an accurate understanding of the microstructure of the nitrided layer on the multiphase stainless steel is essential. In the present work, a hot-rolled stainless steel that has alternating bands of γ-austenite and α-ferrite elongated parallel to the rolling direction was selected as the substrate material for nitridation. Hot-rolled stainless steel is not a usual end product, but its unique banded structure would help reveal the effect of the substrate microstructure on the formation of the nitrided layer.

II. EXPERIMENT DETAILS

The material used in the present work was hot-rolled 304 stainless steel with the chemical composition (wt pct): C 0.07, Si 0.65, Mn 1.49, P 0.004, S 0.009, Cr 17.79, Ni 8.61, Mo 0.05, Ti 0.66, Al 0.13, Fe bal. The samples for plasma nitriding were machined into dimensions of 20 mm × 20 mm × 5 mm from the hot-rolled rod with a diameter of 50 mm. The samples were then ground by using SiC grinding paper down to 1500 grade and polished with diamond paste (mean size 1 μm) before nitriding. Plasma nitriding was carried out by using a DC plasma-nitriding unit (50 kW) at 693 K (420 °C) for 12 hours in a gas of NH_4 at a pressure of 800 to 930 Pa.

The phases present in the nitrided layer were determined by XRD on a Rigaku D/Max-Ultima diffractometer in symmetric Bragg-Brentanno geometry with a Cu Kα radiation (λ = 0.154 nm). Metallographic specimens were chemically etched in a solution of $FeCl_3$ (5 g) + HCl (5 mL) + water (100 mL). Morphological observations were carried out on a Philips XL-30 scanning electron microscope (SEM) and an Olympus GX51 optical microscope (OPM). Additional microstructure analysis was performed on a JEM 2100 transmission electron microscope at a voltage of 200 kV. The specimens for TEM (normal to the rolling direction) were prepared by grinding and mechanical polishing from the untreated side to 40 μm, followed by ion thinning from the untreated side to obtain the thin foil of the nitrided layer surface. The microhardness in various regions was measured with a load of 50 g. Microchemical

composition in various regions was evaluated by energy-dispersive X-ray spectrum (EDS).

III. RESULTS AND DISCUSSIONS

A. *XRD Results*

XRD patterns of the untreated and the nitrided samples are shown Figure 1(a), along with the enlarged figure of the angles (2θ) from 37 to 55 deg for clarity (Figure 1(b)). The results indicated that the untreated sample was composed of γ-austenite and a small amount of α-ferrite and that the peaks were sharp. The peaks of the phase induced by nitriding appeared at lower Bragg angles than those of the substrate austenite, and all were broadened considerably. The peaks of the austenite shifted toward lower Bragg angles, indicating an expansion of the lattice due to nitrogen in the interstitial solution. Therefore, the broad peaks were associated with a metastable phase called "expanded austenite,"
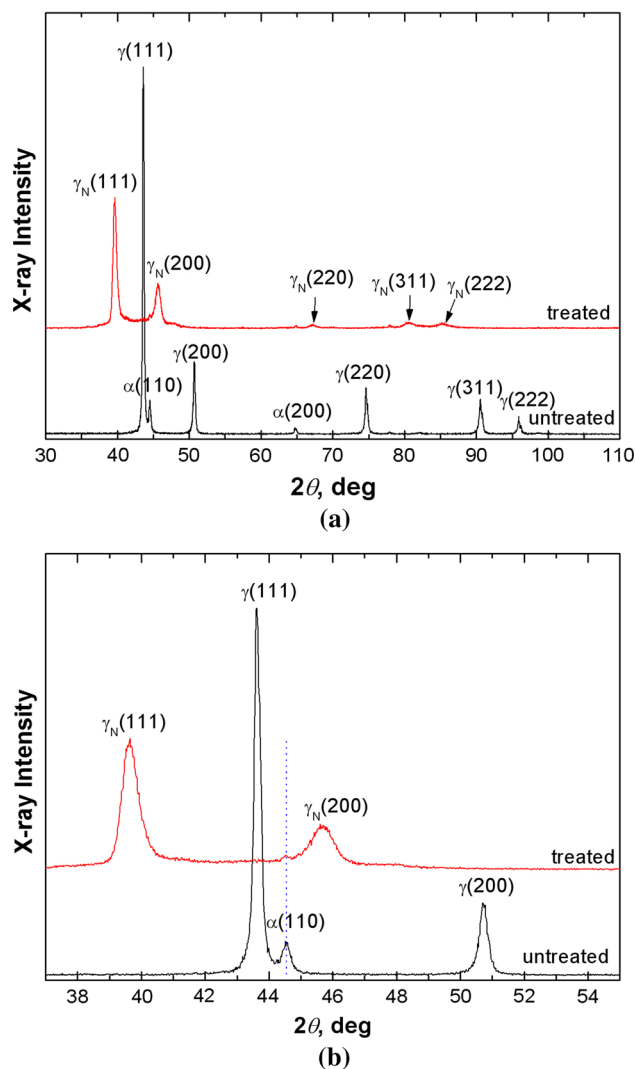

Fig. 1—XRD patterns of untreated and nitrided samples: (*a*) overall pattern and (*b*) enlarged pattern.

Table I. Austenite Lattice Expansion and Nitrogen Content (Atomic Percent)

a (111) (Å)	a (200) (Å)	$\Delta a/a_\gamma$ (111) (Pct)	$\Delta a/a_\gamma$ (200) (Pct)	C_N (avg) (At. Percent)
3.929	3.977	8.5	10.5	43.8

$\Delta a/a_\gamma$ (pct), where $\Delta a = a_{\gamma N} - a_\gamma$.

γ_N, or supersaturated nitrogen austenite.[3–5] Table I shows the relative expansion of the austenite lattice parameter (γ_N) when compared with the untreated austenite, $\Delta a/a_\gamma$ (pct), where $\Delta a = a_{\gamma N} - a_\gamma$. It can be observed that the lattice parameter calculated from the spacing of the (200) plane is higher than that from the (111) plane. The anomalous expansion has been interpreted as tetragonal, monoclinic, and triclinic distortions of the fcc phase.[12,13] Other possibilities included stacking faults or lattice strain due to compressive residual stresses generated by the interstitial nitrogen.[14]

The atomic nitrogen concentration of the expanded austenite C_N can be deduced from the Picard's equation: $a_{\gamma N} = a_\gamma + kC_N$,[18,19] where $a_{\gamma N}$ and a_γ are the unstrained lattice constant of the N-containing layer and the substrate, respectively; and k is the Vegard constant, which is 0.0078 Å per at pct N for pure γ-Fe, which is valid up to a maximum lattice parameter of 0.404 nm.[20] A value of about 43 at. pct was obtained for C_N, which was well above the solubility limit of FCC-austenite (10.3 at. pct) based on the phase diagram.[21] It was implied that a supersaturated nitrogen solid solution in austenite formed in the nitrided layer.

Moreover, determining the lattice spacing with X-ray diffraction methods for a case layer on a substrate is significantly influenced by residual stress in the case layer. For such high nitrogen contents (up to 40 at. pct), the contribution of stresses on the measured lattice parameter can be significant. Additionally, stacking faults, inherent to expanded austenite, would also give rise to a systematic lattice parameter deviancy.[22] However, without knowing the lattice parameter of the stress-free and fault-free γ_N phase in the layer, it is not possible to evaluate accurately the relative contribution of residual stress and stacking fault to the observed peak shift.

It was well understood that the broadening of a diffraction peak is mainly associated with the presence of residual microstress, crystal defects in the specimen, fine grain, or particle size.[23] The microstructure observation in the next section would show that the austenite grain size in the nitrided layer has no obvious change compared with the untreated austenite. Therefore, broadening of the peaks was probably caused by the residual stress by the nitrogen remaining in solid solution in the fcc lattice[2] and the possible defect structure of the nitriding layer.

The peaks of α(110) and α(200) were still detected, but they became weaker. This suggested that the ferrite phase transformed partly into the expanded austenite[10,24] because nitrogen is an austenite stabilizer, or
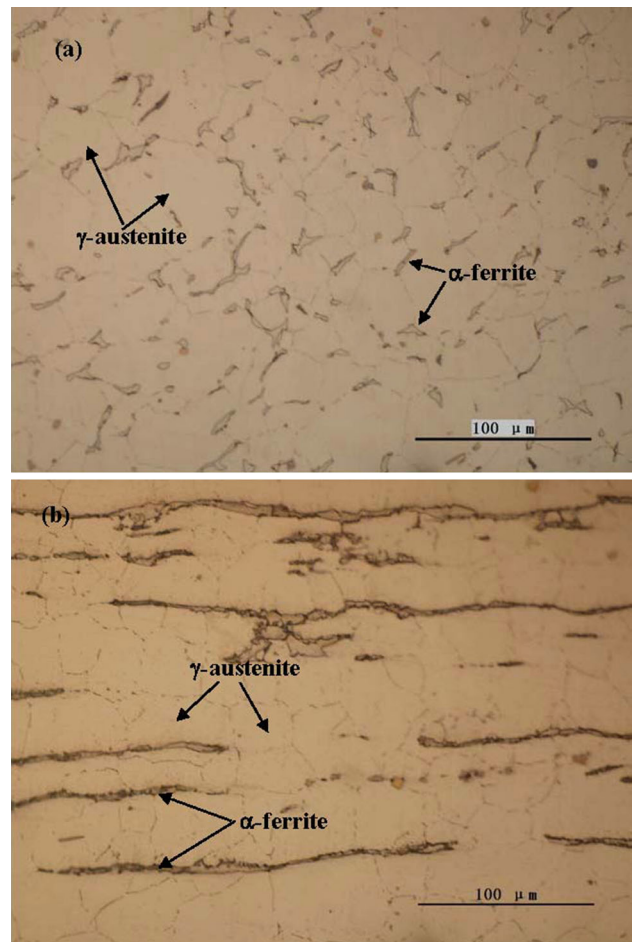

Fig. 2—OPM observation on untreated sample: (a) transverse sample and (b) longitudinal sample.

enlarged the γ-phase zone. Obvious shifting and broadening of the peaks of α-ferrite were not detected. The peaks of chromium-nitride were not found. XRD results seemed to suggest that more nitrogen was introduced into austenite to form a supersaturated fcc iron-nitrogen solid solution or expanded austenite (γ_N) phase but absent of both chromium-nitride precipitation and the supersaturated solid solution of nitrogen in bcc-ferrite (α_N).

B. Microstructure Observations

1. OPM observation

Transverse and longitudinal samples of the hot-rolled stainless steel rod were prepared to reveal the microstructure of the untreated sample. Typical optical micrographs are shown in Figure 2. From the transverse sample, the austenite structure was more or less equiaxed and the grain size varied from 10 to about 50 μm, and approximately 5 pct residual α-ferrite randomly distributed at the austenite boundaries [marked in Figure 2(a)]. From the longitudinal sample, α-ferrite became elongated parallel to the rolling direction to produce a banded structure of alternating γ-austenite and α-ferrite [marked in Figure 2(b)]. Fine intergranular carbides were observed.
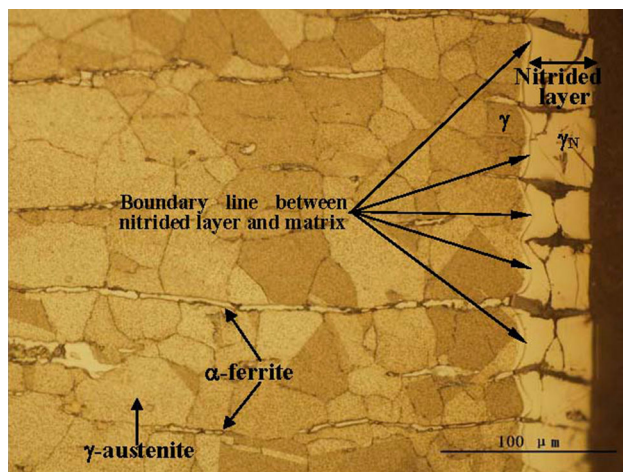
Fig. 3—Optical cross-sectional micrograph of nitrided sample.

Figure 3 shows the cross-sectional OPM micrograph of the nitrided sample. A clear boundary line (a strong etched line marked by arrows in Figure 3) between the nitrided layer and the substrate was observed, but the original banded structure typical of hot-rolled morphology was still present in the nitrided layer. The nitrided layer was composed of "black phases" (dark etched regions) and "white grains" (featureless regions). It was noted that the "black phase" in the nitrided layer was always connected to the elongated α-ferrite in the substrate but that the "white grain" corresponded to the austenite in the substrate. According to the literature, this dark-etched region is mainly composed of chromium nitrides that impair the corrosion resistance.[1,6,8] Interestingly, the boundary line between the nitrided layer and the substrate was zigzag rather than straight (marked in Figure 3), following the alternating distribution of α-ferrite and γ-austenite, which resulted in a continuous varying layer thickness. The average thickness of the nitrided layer was about 40 μm. It was obvious that the "black phase" region corresponded to a deeper diffuse front than the "white grain" region, which was attributed to the different diffusivities of nitrogen in ferrite and austenite. It has been known that nitrogen diffuses faster in bcc ferrite than in fcc austenite.[14,25] It was evident that the formation of the zigzag boundary line also related to the different diffusivities of nitrogen along the α/γ interface and through the lattice.

From Figure 3, it can be observed that the austenite grains in the nitrided layer appeared whitish, while the austenite grains in the substrate were attacked by the etchant used, showing shallow corrosion pits on the surface (very small black corrosion spots in Figure 3). It was suggested that pitting took place on the austenite grains in the substrate by deep etching in the etchant used, but it was absent in the austenite grains in the nitrided layer. This indicated that the supersaturated nitrogen austenite exhibited better corrosion resistance than the austenite in the substrate in the etchant used. A very thin zone free of pitting was found in the substrate close to the nitriding layer, and interestingly, the contour of the zone followed the boundary line between
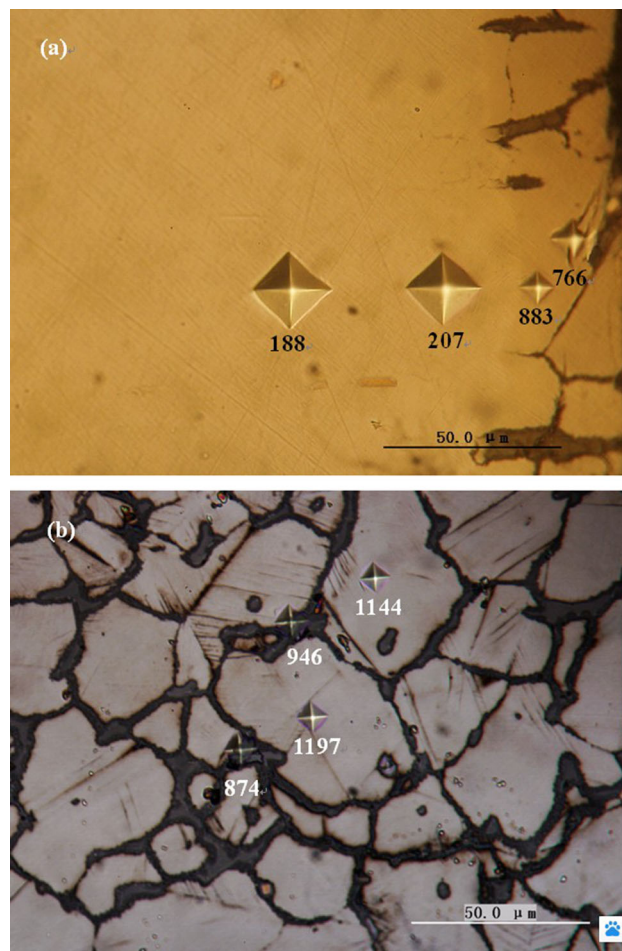

Fig. 4—Microhardness indentation: (a) microhardness profile on cross-sectional nitrided sample and (b) microhardness indentation on nitrided surface.

the nitrided layer and the substrate. It seemed that a double-layer microstructure was present. This feature was observed in nitrided AISI 316[26] and AISI 202 stainless steels,[9] which were described as "outer layer" and "inner layer." EDS analysis later would demonstrate that the "inner layer" was also a nitrogen-rich layer.

The microhardness indentations in various regions are shown in Figure 4. The "white grain" and the "black phase" in the nitrided layer exhibited a much higher hardness relative to the substrate. Additionally, from the nitrided surface [Figure 4(b)], it could be more clearly observed that nitriding did not modify the grain size and shape. However, a lot of slip lines were revealed on the austenite grains. It has been suggested that the surface of the nitrided sample is plastically deformed to induce slip lines on the surface due to high residual stress.[7]

2. SEM observation

The cross-sectional microstructure details of the nitrided layer were studied by SEM [Figures 5(a) and (b)]. It can be observed that the "black phase" in the nitrided layer in the OPM photograph (Figure 3) was composed of two distinct microstructures, the

untransformed elongated structure and the transformed structure (strongly etched regions along the interface between the elongated ferrite and the austenite, marked by fine white arrows in Figure 5). Subsequent TEM observations would demonstrate that the cellular decomposition (mainly $\gamma_N \rightarrow \alpha + CrN$) occurred in the strongly etched regions. The untransformed structure was always associated with the elongated α-ferrite in the substrate, but it was more convex relative to the elongated α-ferrite in the substrate. It was suggested that the ferrite in the nitrided layer exhibited better corrosion resistance than the elongated α-ferrite in the substrate due to the nitrogen introduced. It was interesting that the decomposition precipitations preferentially took place at the α/γ interfaces, along the austenite boundaries, and mainly grew into the austenite grains. A higher magnification SEM micrograph in Figure 5(c) taken in the nitrided layer showed more clearly that dendritic cells of the decomposition product emanated from the α/γ interfaces and that they grew from the austenite boundaries into austenite grains, showing some characteristic features of discontinuous precipitation or cellular decomposition. In classic discontinuous transformation, the cellular precipitations nucleated at preferential sites like grain boundaries and grew into the parent grains.[11,19]

3. Microcomposition evaluation

Semiquantitative elemental analysis in various regions of the nitrided layer [marked in Figure 5(b)] was determined by EDS (Table II). The elemental redistribution revealed enrichment of nitrogen in the austenite and the ferrite of the nitrided layer. Unexpectedly, the nitrogen concentration in the ferrite was more than in the austenite. It is well known that fcc austenite can dissolve more interstitial atoms (C, N) than bcc ferrite due to the large octahedral interstitial sites in fcc structure and that the maximum solubility of nitrogen in austenite and ferrite is 2.86 wt pct [923 K (650 °C)] and 0.10 wt pct [863 K (590 °C)], respectively. It should be mentioned that the smaller electron beam diameter of 500 nm and the lower acceleration voltage of 15 kV were used when doing EDS but that the actual interaction area of electron beam and specimen might exceed the ferrite region in the layer in view of the so-called "pear-shaped effective interaction area." Abnormal excessive nitrogen in the ferrite of the nitrided layer might be partly from the adjacent decomposition regions (strongly etched region). Due to the strong attractive interaction between Cr and N,[8] the nitrogen trapping ability of an octahedral interstice should increase when the fraction of Cr atoms dissolved on the contiguous substutional lattice is increased. Therefore, there was an increase in the nitrogen solubility with chromium content, leading to more nitrogen being readily trapped in the ferrite.[13] It was considered possible that the nitrogen concentration in the ferrite of the nitrided layer was more than the equilibrium solubility limit of the nitrogen in the ferrite at a processing temperature of 693 K (420 °C) after subtracting out the contribution of the adjacent decomposition region. Considering SEM and OPM observations
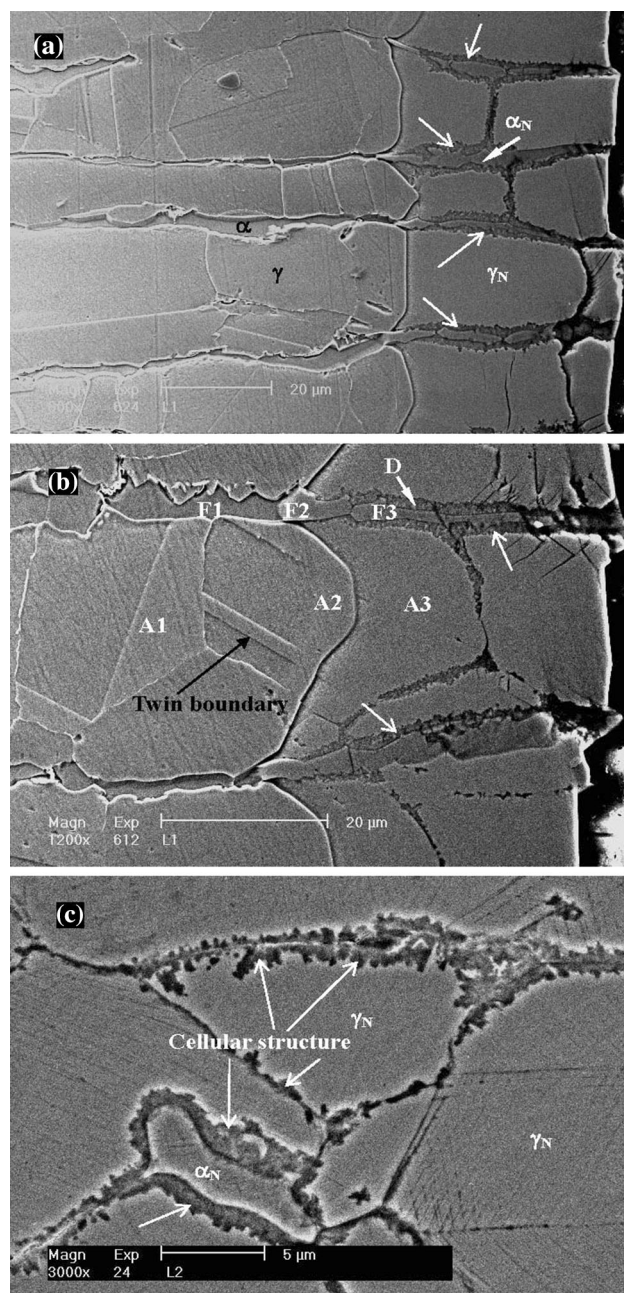

Fig. 5—SEM observation on microstructure of nitrided sample: (a), (b) cross-sectional view and (c) plan view.

and the metastable high solubility of nitrogen effectively created by the chromium, it cannot be excluded that α_N formed in the nitrided layer. Certainly, chromium nitrides would form as long as the chromium mobility is ensured when raising the nitriding temperature and prolonging the nitriding time. Microcomposition analysis by EDS (also shown in Table II) for the major substitutional alloying elements Cr, Ni in stainless steel indicated more content of Cr in the ferrite and Ni in the austenite of the substrate (regions A1 and F1), as expected. Cr concentration in the ferrite of the nitrided layer (region F3) showed an obvious increase when compared with that in the ferrite of the substrate, but Cr

Region	Phase	N	Cr	Ni	Fe
A1	austenite in matrix	/	17.32	9.34	70.20
A2	austenite at interface	4.24	16.87	8.08	69.32
A3	austenite in layer	7.91	16.24	8.39	65.03
F1	ferrite in matrix	/	26.49	3.31	67.28
F2	ferrite at interface	4.35	25.76	2.61	65.84
F3	ferrite in layer	16.59	56.80	2.11	12.86
D	strong etched region	12.36	65.90	0.90	9.83

concentration in the austenite of the nitrided layer (region A3) was almost the same as that in the austenite of the substrate (region A1). The excessive Cr in the ferrite of the nitrided layer also might come from the adjacent decomposition region as in the previous discussion. In the strongly etched region (region D), a marked increase of Cr and a decrease of Ni and Fe were observed in accordance with the fact that Cr are strong nitride-forming elements, whereas Ni is not. TEM observations later would demonstrate that a discontinuous precipitation reaction occurred in the strongly etched regions to form a lamellar structure of CrN + α. EDS evaluation indicated that the nitrogen enrichment took place in the very thin "inner layer" (regions F2 and A2) when compared with the inward substrate.

4. TEM observation

A typical microstructure of the untreated sample and corresponding SADPs are shown in Figure 6. The SADPs (Figures 6(b) and (c)) demonstrated that the substrate was mainly composed of γ-austenite and α-ferrite, which corresponded with the XRD result. It was noted that additionally spots were presented in both diffraction patterns and these were mostly likely due to aligned oxide films on the upper and lower surfaces of the TEM foils [indexed in Figure 6(c)] and to corresponding double diffraction spots [shown by arrows in Figure 6(b)]. The microstructure revealed a very high density of dislocations[27] (Figure 6(a)) as expected of rolled stainless steel. Additionally, rod-like carbides were found at the grain boundaries, which corresponded with the OPM observation.

TEM observation indicated that the nitrided layer exhibited two distinct microstructures in general, the decomposition region consisting of lamellae-like precipitates and the nonlamellar region (Figure 7).

As observed by SEM, phase interfaces (the α/γ) and the austenite grain boundaries were decorated with the cellular decomposition products (Figures 7(a) and (b)). The cellular decomposition products predominately emanated from the α/γ interfaces, which existed along the austenite grain boundaries, and mainly grew into the austenite grains and occasionally into the ferrite grains [marked by an arrow in Figure 7(b)]. It was noted that the cells that had nucleated independently impinged on one another during their growth (Figure 7(c)). Many SADPs from regions containing these decomposition products with fine interlamellar spacings showed that strong spot patterns from the ferrite always had some weak spots (Figure 7(e)) or discontinuous rings (not shown in this article) that were identified as from the CrN. The patterns indicated α-ferrite and CrN to be the decomposition products. It was suggested that the decomposition reaction of $\gamma_N \rightarrow \alpha + CrN$ occurred. The lamellae continued to grow, and the establishment of unique lamellar spacing was mainly achieved by branching of the existing lamellae at the advancing interface.[9] When a regular interlamellar spacing and coarse lamellae were observed to exist (Figure 7(c)), the two sets of integrated crystal spot pattern were obtained (Figure 7(f)). The SADP results indicated that they were α-ferrite and CrN and that the orientation relationship between the two phases was $(100)_{CrN}//(100)_{\alpha}$; $[011]_{CrN}//[001]_{\alpha}$, which corresponded with the Baker–Nutting relationship.[28] It was noted that the extent of decomposition in different grains varied widely. For example, in some grains, the cellular precipitates had exhibited regular cooperative growth and a unique lamellar spacing was achieved, as shown in Figure 7(c). However, in other grains, the cellular reaction was found to be in its initial stages, as shown in Figure 7(a). Such wide variation in the rate of the cellular reaction can be attributed to the difference in mobility of the grain boundaries.[28,29]

Usually, independent nucleation of cells occurs on the high-angle grain boundaries and the development of the cellular structure has been attributed to the bowing of the mobile grain boundary that is pinned by the presence of discrete equilibrium precipitates.[30] Electron back-scattered diffraction (EBSD) studies revealed that the discontinuous precipitation growth was also governed by specific crystallographic considerations.[28] The formation of nitrides in the nitriding process was mainly controlled by the diffusion of the metal atoms; therefore, the cellular precipitation at the α/γ interface suggested that the interface acted as a heterogeneous nucleation site and as an enhanced diffusion path. Although nucleation at the boundaries was dominated, there was also evidence for nucleation within the grains (Figure 7(d)), which might be attributed to the presence of some lattice defects, such as vacancies as a preferred heterogeneous nucleation site.

Within a single ferrite grain apparently containing few such decomposition products (the nonlamellar region), a single crystal pattern was obtained. However, it was noticeable that in the present study, a bcc crystal pattern was frequently found, such as SADP in Figure 7(g), which came from the nonlamellar region in Figure 7(b). EDP in Figure 7(g) has identical zone axes with EDP of ferrite in Figures 7(e) and (f) from the decomposition
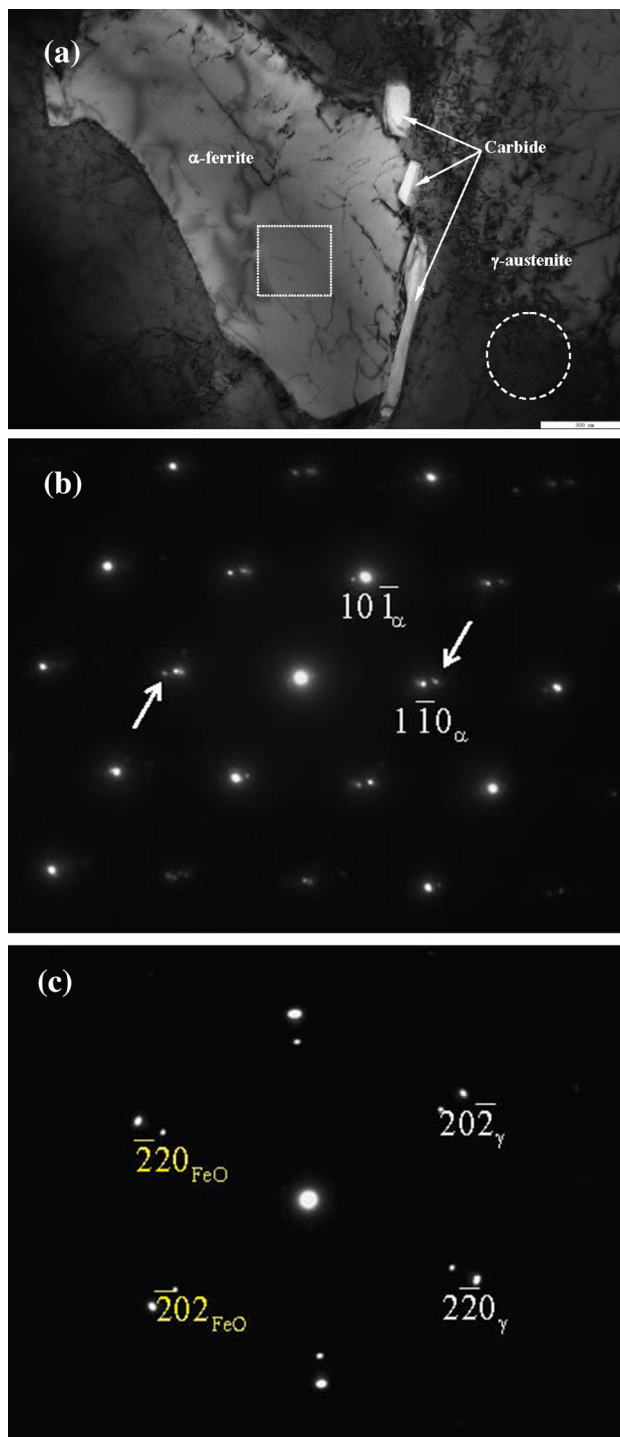
Fig. 6—TEM observation on untreated sample: (*a*) Microstructure, (*b*) SADP of α-ferrite, boxed region in (*a*), and (*c*) SADP of γ-austenite, circled region in (*a*).

diffused intensity maxima in their EDP.[31,32] These data and interpretations did not exclude that the initial stage of precipitation comprised a substitutional—interstitial solute—atom clustering. In view of a stronger attractive interaction between Cr and N than Fe and N or Ni and N,[8] the detectable nitrogen content in the nitrided ferrite higher than the equilibrium solubility limit of nitrogen in the ferrite, and its better corrosion resistance compared with the ferrite in the substrate, it was suggested that a supersaturated nitrogen solid solution based on a bcc ferrite with Cr-N clusters or pairs in short-range ordering, α_N, formed in the nitrided layer. As expected, an fcc single crystal pattern was also found (Figure 7(h)), whose spots also exhibited intense diffused scattering.[33] The fcc single crystal was typical of expanded austenite (γ_N) described in previous literature.[2,4] With Au-calibrated camera constant (Lλ), no obvious lattice expansion was detected from the bcc and fcc phases. It must also be mentioned that it was difficult to determine accurately the lattice parameter of γ_N and α_N due to the strong diffuse intensity of the diffraction spots from EDPs. The lattice expansion of γ_N from XRD results was about 9 to 10 pct, which showed obvious inconsistency with the EDP result. Therefore, the shift of XRD peaks of γ_N was more closely related to the residual stress in the nitrided layer because the residual stress has been fully released during TEM specimen preparation. It was noted that both γ_N and α_N exhibited very different microstructures from α-ferrite and γ-austenite in the untreated sample. They showed little diffraction contrast (Figures 7(a) through (d)) when compared with α-ferrite and γ-austenite in the untreated sample (Figure 6(a)). This monotonous contrast was most probably attributed to "structure-factor contrast" reflective of solute atoms segregation.[34] If there are small crystals of different atoms in a given foil, the difference in their structure-factor (F_{hkl}) from that of the matrix would cause contrast changes. The presence of very small-size clusters of atom segregation would be detected in this way. The monotonous contrast was considered to have the characteristic of an amorphous phase contrast to some extent by many literatures.[6,35,36] Due to the low mobility of the Cr atoms as compared with the interstitials N at the low treatment temperature, the precipitation of chromium nitrides is effectively prevented. The high interstitial content of nitrogen is obtained because of the relatively strong attractive interaction between Cr atoms and N atoms, leading to anticipated short-range ordering of Cr and N. The Cr-N pairs or clusters in the supersaturated solid solution contributed to the "structure factor contrast" and corresponding diffuse effect of electron diffraction spots. In recent research,[6] the lack of the crystallinity (amorphous-like contrast) of γ_N was also attributed to the effect of the massive introduction of nitrogen/carbon into the austenite matrix, which is associated with the low diffusivity of substitutional alloying elements, such as chromium and molybdenum. The massive introduction of nitrogen into the austenite (maybe into the ferrite) was confirmed by EDS in the present work. The presence of so-called "stacking fault precipitates" and the "deformed twins"[12,33] in γ_N were prominent

regions in Figures 7(b) and (c). However, it can be distinctly observed that the spots from the single ferrite grain (Figure 7(g)) showed an obvious diffuse scattering effect in the form of broadening and trailing of the fundamental reflections. Solid solutions with short-range order of alloy element clusters or pre-precipitation and short-range order of vacancies[31] usually exhibit
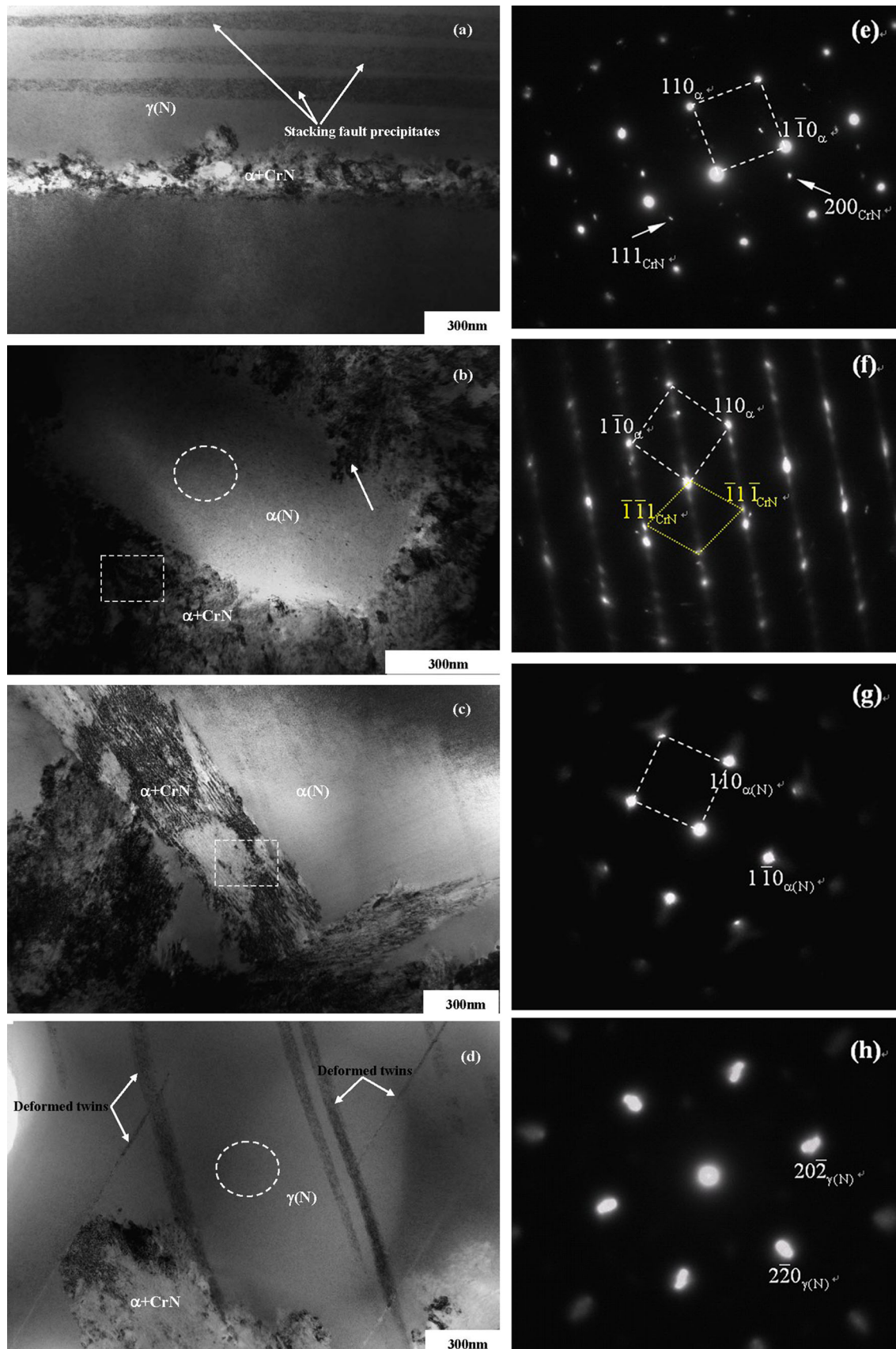
Fig. 7—TEM observation on nitrided layer: (*a*), (*b*) lamellar structure along the boundary; (*c*) coarse lamellar structure; (*d*) lamellar structure within the grain; (*e*) EDP of lamellar structure, boxed region in (b); (*f*) EDP of lamellar structure, boxed region in (c); (*g*) nonlamellar structure, circled region in (b); and (*h*) nonlamellar structure, circled region in (d).

features of its microstructure [marked in Figures 7(a) and (d)], but the absence of α_N was attributed to lower stacking fault energy and more slip systems of fcc austenite. The formation of such "defects" may be facilitated since N was known to reduce the fault stacking energy in austenite.[37] From the microstructure features of the nitrided layer and their SADPs, the following discontinuous precipitation reaction primarily took place: $\gamma_N \rightarrow \alpha + CrN$, initiating from the α/γ interfaces beside the grain boundaries of austenite.[8,38,39] General characteristics of classic discontinuous precipitation are as follows:[38]

(1) The morphology of the discontinuous precipitation is lamellae-like.
(2) The reaction takes place in supersaturated grains containing continuous precipitates.
(3) The initiation of the reaction requires mobile grain boundaries.

With regard to these characteristics, the present experiments provided the following results:

(1) The lamellae-like structure was revealed by TEM (Figure 7) and SEM (Figure 5).
(2) The presence of continuous precipitates was indicated by very high microhardness values of γ_N and the formation of γ_N with Cr-N pairs or clusters (demonstrated by the diffuse scattering effect in their SADPs and "structure factor contrast" in the TEM microstructure).
(3) SEM and TEM observations showed that the discontinuous precipitation reaction was initiated at the α/γ interfaces and the austenite boundaries. Nitriding proceeded faster along the phase interfaces or the grain boundaries than through the lattice.

The extent of discontinuous precipitation at the α/γ interfaces was more pronounced than at the austenite boundaries. The chromium content in α-ferrite was higher than that in γ-austenite; therefore, the excessive chromium facilitated to precipitation of CrN. It was suggested that the extent of the discontinuous precipitation was closely related to the chromium content.

IV. CONCLUSIONS

1. The nitrided layer was mainly composed of the supersaturated solid solution of nitrogen in austenite (γ_N). The microstructure of γ_N exhibited "structure factor contrast," and the corresponding EDPs revealed a strong diffuse scattering effect, reflective of an occurrence of small pre-precipitation with additional short-range order Cr-N pairs or clusters in γ_N. γ_N exhibited better corrosion resistance than γ-austenite in the substrate.
2. The occurrence of a supersaturated solid solution of nitrogen in ferrite (α_N) in the nitrided layer was not excluded, in view of the microstructural features similar γ_N revealed in the ferrite of the nitrided layer, and its better corrosion resistance than ferrite in the substrate.

3. Discontinuous precipitations of $\gamma_N \rightarrow \alpha + CrN$ occurred predominantly at the γ/α interfaces, and it grew from the austenite boundaries into austenite grains, forming a lamellae structure consisting of CrN and α-ferrite. The orientation relationship between CrN and α-ferrite corresponded to a Baker-Nutting relationship: $(100)_{CrN}//(100)_\alpha$; $[011]_{CrN}//[001]_\alpha$.
4. A zigzag boundary line following the banded structure of alternating γ-austenite and elongated α-ferrite was presented between the nitrided layer and the substrate, resulting in continuous varying layer thickness. This was attributed to different diffusivities of nitrogen in ferrite and in austenite, along the α/γ interface and through the lattice.

ACKNOWLEDGMENTS

REFERENCES

1. Y. Sun, X.Y. Li, and T. Bell: *J. Mater. Sci.*, 1999, vol. 34, pp. 4793–02.
2. M.P. Fewell, D.R.G. Mitchell, J.M. Priest, K.T. Short, and G.A. Collins: *Surf. Coats. Technol.*, 2000, vol. 131, pp. 300–306.
3. M. Samandi, B.A. Shedden, D.I. Smith, G.A. Collins, R. Hutchings, and J. Tendy: *Surf. Coats. Technol.*, 1993, vol. 59, pp. 261–66.
4. D.L. Williamson, O. Ozturk, R. Wei, and P.J. Wilbur: *Surf. Coats. Technol.*, 1994, vol. 65, pp. 15–23.
5. A. Saker, Ch. Leroy, H. Michel, and C. Frantz: *Mater. Sci. Eng.*, 1991, vol. 140A, pp. 702–708.
6. F.A.P. Fernandes, L.C. Casteletti, and J. Gallego: *J. Mater. Res. Technol.*, 2013, vol. 2, pp. 158–64.
7. M. Asgari, A. Barnoush, R. Johnsen, and R. Hoel: *Mater. Sci. Eng., A*, 2011, vol. 529, pp. 425–34.
8. J. Wang, Y. Lin, J. Yan, D. Zen, Q. Zhang, R. Huang, and H. Fan: *Surf. Coat. Technol.*, 2012, vol. 206, pp. 3399–4304.
9. F. Borgioli, A. Fossati, G. Matassini, E. Galvanetto, and T. Bacci: *Surf. Coat. Technol.*, 2010, vol. 204, pp. 3410–17.
10. R. Huang, J. Wang, S. Zhong, M. Li, J. Xiong, and H. Fan: *Appl. Surf. Sci.*, 2013, vol. 271, pp. 93–97.
11. N. Granito, H. Kuwahara, and T. Aizawa: *J. Mater. Sci.*, 2002, vol. 47, pp. 835–44.
12. H. Dong, M. Esfandiari, and X.Y. Li: *Surf. Coat. Technol.*, 2008, vol. 202, pp. 2969–75.
13. A.M. Kliauga, M. Pohl, C. Cordier-Robert, and J. Foct: *J. Mater. Sci.*, 1999, vol. 34, pp. 4065–73.
14. C. Blawert, A. Weisheit, B.L. Mordike, and F.M. Knoop: *Surf. Coat. Technol.*, 1996, vol. 85, pp. 15–27.
15. C. Blawert, B.L. Mordike, Y. Jirásková, and O. Schneeweiss: *Surf. Coat. Technol.*, 1999, vols. 116–119, pp. 189–98.
16. F. Bottoli, G. Winther, T.L. Ghristiansen, and M.A.J. Somers: *Metall. Trans. A*, 2015, vol. 46A, pp. 2591–97.
17. S.K. Kim, J.S. Yoo, J.M. Priest, and M.P. Fewell: *Surf. Coat. Technol.*, 2003, vols. 163–1164, pp. 380–85.
18. K. Marchev, C.V. Copper, J.T. Blucher, and B.C. Giessen: *Surf. Coat. Technol.*, 1998, vol. 99, pp. 255–58.
19. K. Marchev, R. Hidalgo, M. Landis, R. Vallerio, C.V. Copper, and B.C. Giessen: *Surf. Coat. Technol.*, 1999, vol. 112, pp. 67–70.
20. O. Celik, M. Baydoban, E. Atar, E.S. Kayali, and H. Cimenoglu: *Mater. Sci. Eng.*, 2013, vol. 565, pp. 38–43.

21. V. Raghavan: *J. Phase Equilibria*, 1997, vol. 18, pp. 158–72.
22. T. Christiansen and M.A.J. Somers: *Metall. Trans. A*, 2007, vol. 37A, pp. 675–82.
23. B.D. Cullity and S.R. Stock: *X-ray Diffraction*, Prentice-Hall, Englewood Cliffs, NJ, 2001, pp. 281–89.
24. Z. Yu, X. Xu, L. Wang, J. Qiang, and Z. Hei: *Surf. Coat. Technol.*, 2002, vol. 153, pp. 125–30.
25. B. Larisch, U. Brusk, and H.-J. Spies: *Surf. Coat. Technol.*, 1999, vols. 116–119, pp. 205–211.
26. F. Borgioli, A. Fossati, E. Galvanetto, T. Bacci, and G. Pradelli: *Surf. Coat. Technol.*, 2006, vol. 200, pp. 5505–531.
27. D.R.G. Mitchell, D.J. Attard, G.A. Collins, and K.T. Short: *Surf. Coat. Technol.*, 2003, vol. 165, pp. 107–18.
28. M. Sennour, P.H. Jouneau, and C. Esnouf: *J. Mater. Sci.*, 2004, vol. 39, pp. 4521–31.
29. D.Q. Peng, T.H. Kim, J.H. Chung, and J.K. Park: *Appl. Surf. Sci.*, 2010, vol. 256, pp. 7522–29.
30. M. Vijayalakshmi, V. Seetharman, and V.S. Raghunathn: *Acta Metall.*, 1982, vol. 30, pp. 1147–56.
31. J.W. Edington: *Practice Electron Microscopy in Materials Science (Part II)*, The Macmillan Press, London, U.K., 1975, pp. 102–05.
32. K.A. Tayor, G.B. Olson, M. Cohen, and J.B. Vander: Sande*Metall. Trans. A*, 1989, vol. 20A, pp. 2749–62.
33. X. Xu, L. Wang, Z. Yu, J. Qiang, and Z. Hei: *Metall. Trans. A*, 2000, vol. 31A, pp. 1193–99.
34. D.B. Williams and C.B. Carter: *Transmission Electron Microscopy: A Textbook for Materials Science*, 2nd ed., Springer, New York, NY, 2009, p. 354.
35. X. Li, M. Samandi, D. Dunne, G. Collins, J. Tendys, K. Short, and R. Hutchings: *Surf. Coat. Technol.*, 1996, vol. 85, pp. 28–36.
36. L. Hisang, S.-C. Chen, and C.-Z. Wu: *Appl. Surf. Sci.*, 2011, vol. 257, pp. 7375–80.
37. E.I. Meletis, V. Singh, and J.C. Jiang: *J. Mater. Sci. Lett.*, 2002, vol. 21, pp. 1171–74.
38. P.M. Hekker, H.C.F. Rozendaal, and E.J. Mitteneijer: *J. Mater. Sci.*, 1985, vol. 20, pp. 718–29.
39. L. Nosei, M. Avalos, B.J. Gómez, L. Nachez, and J. Feugeas: *Thin Solid Film*, 2004, vol. 468, pp. 134–41.